



Direct detection of natural selection in Bronze Age Britain

Iain Mathieson and Jonathan Terhorst

Genome Res. published online October 31, 2022

Access the most recent version at doi:[10.1101/gr.276862.122](https://doi.org/10.1101/gr.276862.122)

P<P	Published online October 31, 2022 in advance of the print journal.
Accepted Manuscript	Peer-reviewed and accepted for publication but not copyedited or typeset; accepted manuscript is likely to differ from the final, published version.
Creative Commons License	This article is distributed exclusively by Cold Spring Harbor Laboratory Press for the first six months after the full-issue publication date (see https://genome.cshlp.org/site/misc/terms.xhtml). After six months, it is available under a Creative Commons License (Attribution-NonCommercial 4.0 International), as described at http://creativecommons.org/licenses/by-nc/4.0/ .
Email Alerting Service	Receive free email alerts when new articles cite this article - sign up in the box at the top right corner of the article or click here .

Comprehensive immune receptor profiling.
Discover the **DriverMap™ AIR Assay** difference.



To subscribe to *Genome Research* go to:
<https://genome.cshlp.org/subscriptions>

Published by Cold Spring Harbor Laboratory Press

1 Direct detection of natural selection in Bronze Age Britain

2 Iain Mathieson¹ and Jonathan Terhorst²

3 ¹Department of Genetics, Perelman School of Medicine, University of Pennsylvania

4 ²Department of Statistics, University of Michigan

5 August 23, 2022

6 Correspondence to I.M. mathi@pennmedicine.upenn.edu or J.T. jonth@umich.edu.

7 **Abstract**

8 We developed a novel method for efficiently estimating time-varying selection coef-
9 ficients from genome-wide ancient DNA data. In simulations, our method accurately
10 recovers selective trajectories, and is robust to mis-specification of population size. We
11 applied it to a large dataset of ancient and present-day human genomes from Britain,
12 and identified seven loci with genome-wide significant evidence of selection in the past
13 4500 years. Almost all of them can be related to increased vitamin D or calcium lev-
14 els, suggesting strong selective pressure on these or related phenotypes. However, the
15 strength of selection on individual loci varied substantially over time, suggesting that
16 cultural or environmental factors moderated the genetic response. Of 28 complex an-
17 thropometric and metabolic traits, skin pigmentation was the only one with significant
18 evidence of polygenic selection, further underscoring the importance of phenotypes
19 related to vitamin D. Our approach illustrates the power of ancient DNA to charac-
20 terize selection in human populations and illuminates the recent evolutionary history
21 of Britain.

22 Introduction

23 Ancient DNA (aDNA) provides direct insight into human evolutionary history. So far, this
24 information has mainly been used to study demographic history—the migrations, splits and
25 admixtures that humans experienced in the recent past (Skoglund and Mathieson, 2018).
26 But in principle, aDNA can also tell us about phenotypic evolution and, in particular,
27 about the contribution of natural selection to phenotypic and genomic variation. Compared
28 to demographic inference, this is more challenging, because studies of natural selection
29 typically require larger sample sizes than studies of population history, which can integrate
30 information from across the genome.

31 Although some recent studies have used aDNA to study selection and phenotypic evolu-
32 tion, they have mostly focused on a relatively small number of loci (e.g., Wilde et al., 2014;
33 Mathieson and Mathieson, 2018; Kerner et al., 2021). Studies that performed genome-wide
34 scans for selection using aDNA (Mathieson et al., 2015; Skoglund et al., 2017; Margaryan
35 et al., 2020) have compared allele frequencies across populations, but have not made use of
36 the precise temporal information available from direct dating of ancient samples. For ex-
37 ample, the approach in Mathieson et al. (2015) was able to detect selection that happened
38 some time in the past 8,000 years, somewhere in Western Eurasia, but could not be more
39 specific.

40 With the recent publication of large aDNA datasets (e.g., Patterson et al., 2022; Olalde
41 et al., 2019; Margaryan et al., 2020), sample sizes for some regions are now in the hundreds
42 of individuals, large enough to study selection with good spatial and temporal resolution.
43 However, there is a lack of suitable methods to analyze these data. There are many pub-
44 lished methods for estimating selection coefficients from time series data (e.g., Bollback
45 et al., 2008; Malaspina et al., 2012; Mathieson and McVean, 2013; Lacerda and Seoighe,
46 2014; Feder et al., 2014; Steinrücken et al., 2014; Terhorst et al., 2015; Tataru et al., 2017),
47 but all of them unrealistically assume that selective pressures are constant over time, and
48 most are too slow to run on millions of markers at once. We therefore developed a novel

49 statistical approach which is able to estimate arbitrary time-varying selection coefficients,
50 while being fast enough to run genome-wide.

51 The population of Britain, from 4500 years before present (BP, i.e. the start of the
52 Bronze Age) to the present-day is ideal to demonstrate this approach for several reasons.
53 First, it is relatively homogeneous in terms of both genetics and environment. Second, it
54 is the population with the largest aDNA sample size. Third, there is a large amount of
55 data about the genetic basis of complex traits in this population due to analysis of the
56 UK Biobank. Finally, one of the few studies that attempted to detect selection over this
57 time period (based on data from present-day individuals) was performed in this population
58 ([Field et al., 2016](#)), giving us a point of comparison for our aDNA-based approach.

59 Methods

60 We begin by formally defining the data, the inference problem, and the model we used
61 to solve it. Our model is a generalization of the one used in ([Mathieson and McVean,
62 2013](#)). We assume a haploid Wright-Fisher population model whose size t generations
63 before present was $2N_t$. Time runs backwards, so that $t = 0$ is the present, and $t = T$ is
64 the earliest point where we have data. We are interested in the frequency of a single allele
65 with two types A and a . In generation t , the a allele has relative fitness $1 + s_t/2$ relative to
66 A . Our inferential target is the vector $\mathbf{s} = (s_0, \dots, s_T)$ of selection coefficients over time.
67 The population size history (N_0, \dots, N_T) is also allowed to vary with time, but we assume
68 that it is known and do not attempt to jointly estimate it with \mathbf{s} .

69 The data consist of pairs of counts $\{(a_t, n_t)\}_{t=0}^T$. Each pair $(a_t, n_t) \in \mathbf{Z}_{\geq 0}^2$ represents
70 the number a_t of a alleles observed out of n_t samples collected t generations ago. Missing
71 data or generations where no sampling occurred are indicated by setting $n_t = 0$. Our model
72 conditions on the sample sizes n_t , and we suppress notational dependence on them going
73 forward.

74 The data generating model is as follows. At time t , let the (unobserved) population

75 frequency of the a allele be $f_t \in [0, 1]$. Given f_t , the data in generation t are binomially
 76 distributed with success probability f_t :

$$a_t | f_t \sim \text{Binom}(n_t, f_t). \quad (1)$$

77 The latent allele frequency trajectory $\mathbf{f} = (f_0, f_1, \dots, f_T)$ evolves according to a Wright-
 78 Fisher (WF) model with genic selection and no mutation (e.g., [Ewens, 2004](#)). Given f_t and
 79 s_t , the number of individuals $F_{t-1} \in [0, 2N_{t-1}]$ possessing the a allele in next generation
 80 has distribution

$$F_{t-1} | f_t, s_t \sim \text{Binom}(2N_{t-1}, f'_t), \quad \text{where } f'_t = \frac{(1 + s_t/2)f_t}{1 + s_t f_t/2}, \quad (2)$$

81 and then we set $f_{t-1} = F_{t-1}/(2N_{t-1})$.

82 Let $\mathbf{a} = (a_0, \dots, a_T)$ denote the data. The complete likelihood is

$$p_{\mathbf{s}}(\mathbf{a}, \mathbf{f}) = \pi_T(f_T) p(a_T | f_T) \prod_{t=0}^{T-1} p(a_t | f_t) p_{\mathbf{s}}(f_t | f_{t+1}), \quad (3)$$

83 where $\pi_T(f_T)$ is a prior distribution on the initial allele frequency (described in more detail
 84 below), and the probabilities $p_{\mathbf{s}}(f_t | f_{t+1})$ and $p(a_t | f_t)$ are specified by (1)–(2). (Through-
 85 out this section, we use the notation $p_{\mathbf{s}}$ to denote probability distributions that depend on
 86 the selection parameters \mathbf{s} .) The likelihood of the observed data is obtained by marginal-
 87 izing (3) over \mathbf{f} :

$$p_{\mathbf{s}}(\mathbf{a}) = \int_{\mathbf{f}} p_{\mathbf{s}}(\mathbf{a}, \mathbf{f}). \quad (4)$$

88 By exploiting the Markov structure of (3), the integral (4) can be efficiently evaluated
 89 using the forward algorithm. Each step of the forward algorithm costs $\mathcal{O}(N_{t-1}N_t)$ owing the
 90 need to evaluate the transition probability (2) for all possible values of f_{t-1} and f_t . When
 91 the effective population size is large (greater than 10^3 , say) this quadratic scaling causes
 92 computation to become slow, and it is advantageous to model the latent allele trajectory
 93 f_t using a continuous approximation. Several have been proposed, including using the
 94 WF diffusion ([Bollback et al., 2008](#); [Malaspinas et al., 2012](#); [Lacerda and Seoighe, 2014](#);

95 Steinrücken et al., 2014; Ferrer-Admetlla et al., 2016); Gaussian approximations to the
96 WF model (Mathieson and McVean, 2013; Lacerda and Seoighe, 2014; Feder et al., 2014;
97 Terhorst et al., 2015); and approximations based on the beta distribution (Tataru et al.,
98 2017, 2015; Gompert, 2016). See also Malaspinas (2016) and references therein. A recent
99 review (Paris et al., 2019) found the beta-with-spikes (hereafter, BWS) approximation of
100 Tataru et al. (2017) to perform consistently better than other approaches, so we use it as
101 our starting point.

102 In this model, the latent frequency $f_t \in [0, 1]$ of the selected allele is modeled as a
103 mixture distribution with three components. There are two atoms at $f_t = 0$ and $f_t = 1$ to
104 allow for the possibility of allele loss or fixation, and the third component is a beta density
105 characterizing the intermediate frequencies, $f_t \in (0, 1)$. The form of this model is motivated
106 by the fact that, in the original WF process, the probability of loss or fixation is positive,
107 whereas it is zero if f_t possesses an absolutely continuous density.

108 Although the BWS model is state-of-the-art, room for improvement remains. Paris
109 et al. (2019) found that, while generally accurate, the BWS approximation degrades when
110 selection is strong and the effective population size is small. Crucially, we cannot necessarily
111 rule such a regime out when analyzing aDNA data. Another potential shortcoming, not
112 reported by Paris et al. but encountered when we implemented the BWS model, concerns
113 the method used to approximate the transition probability

$$p(f_{t+\Delta t} = y \mid f_t = x, N_t, s_t). \quad (5)$$

114 We found that errors in the moment recursions used to compute these probabilities (eqn. (6)
115 onwards of Paris et al., 2019) tended to accumulate, leading to numerical instability and
116 situations where the variance of the resulting beta approximation, or the spike probabilities,
117 were sometimes computed to be negative. (Python code illustrating this phenomenon is
118 included as Supplemental Code S1.) This led us to consider refinements of the BWS model.

119 Beta mixture model

120 Breakdown of the moment-based approximation can be explained by insufficient degrees
 121 of freedom. The two-parameter beta distribution is not flexible enough to accurately ap-
 122 proximate the density (5) in all cases. A potential solution is to enrich the approximating
 123 class of distributions, by modeling the continuous component of (5) as a *mixture* of beta
 124 distributions. This solution is intuitive, and also has theoretical justification: by a famous
 125 result of Bernstein (e.g., Feller, 2008), it holds for any continuous function $g : [0, 1] \rightarrow \mathbf{R}$
 126 that

$$g(x) = \lim_{M \rightarrow \infty} \sum_{m=0}^M g(m/M) b_{m,M}(x), \quad \text{uniformly,} \quad (6)$$

127 where $b_{m,M}$ is proportional to the $\text{Beta}(m+1, M-m+1)$ density. Hence, by taking M
 128 on the right-hand side of (6) to be large but finite, we can accurately approximate any
 129 absolutely continuous density on the unit interval. We refer to this model as the *Beta-*
 130 *mixture-with-spikes* (BMwS). A schematic of our model, which accompanies the discussion
 131 in the next few subsections, is shown in Figure 1.

132 Under BMwS, the (posterior) density of f_t is modeled as a mixture of M beta densities,
 133 plus two atoms at $f_t = 0$ and $f_t = 1$. We abuse notation slightly and write this as

$$f_t \sim p_{t0} \delta_0 + p_{t1} \delta_1 + (1 - p_{t0} - p_{t1}) \sum_{m=0}^M c_{tm} \text{Beta}(\alpha_{tm}, \beta_{tm}), \quad (7)$$

134 where δ_x denotes a point mass at x , and M is a user-specified parameter which trades
 135 approximation accuracy for speed. To model allele frequency trajectories, we need to char-
 136 acterize the distribution of f_{t-1} when f_t has the distribution (7). We follow earlier work
 137 in utilizing a moment-based approximation, however the form of approximation is new.
 138 Previously (e.g., Lacerda and Seoighe, 2014; Terhorst et al., 2015; Tataru et al., 2017; Paris
 139 et al., 2019), the mean and variance of f_{t-1} were obtained by Taylor expansion about the
 140 infinite-population (zero variance) allele frequency trajectory, and then a moment-matched
 141 Gaussian or beta distribution was used to approximate the distribution of f_{t-1} . Here we

142 proceed differently, by directly modeling the action of the WF transition kernel on a beta-
143 distributed random variable.

144 Assume first that $f_t \sim \text{Beta}(\alpha, \beta)$, and let f'_t and f_{t-1} be as in (2). Using a computer
145 algebra system, we determined that

$$\mathbf{E}f_{t-1} \approx \frac{\alpha(2\alpha + \beta(s+2) + 2)}{2(\alpha + \beta)(\alpha + \beta + 1)} \quad (8)$$

$$\text{var } \mathbf{E}(f_{t-1} | f'_t) \approx \frac{\alpha\beta(\alpha(1-s) + \alpha + \beta s + \beta + 2)}{(\alpha + \beta)^2(\alpha + \beta + 1)(\alpha + \beta + 2)} \quad (9)$$

$$\mathbf{E} \text{var}(f_{t-1} | f'_t) \approx \frac{\alpha\beta(\alpha(2-s) + \beta(s+2) + 4)}{4N_{t-1}(\alpha + \beta)(\alpha + \beta + 1)(\alpha + \beta + 2)}. \quad (10)$$

146 (A Mathematica notebook verifying these computations is included as Supplemental Code
147 S2.) These approximations are obtained by Taylor expansion of f'_t about $s = 0$, followed
148 by substituting in moments of the beta distribution. It would be easy to extend them to
149 higher powers of s , but we did not find it necessary, since $|s| = 0.1$ is already at the extreme
150 end of what we expect to find in natural data. Note that for $|s| < 1$ (at least), the above
151 equations imply $\text{var } f_{t-1} > 0$, so this approximation is robust to the pathology described
152 above.

153 Using (8)–(10), we can find α', β' such that f_{t-1} has approximately a $\text{Beta}(\alpha', \beta')$ dis-
154 tribution:

$$\alpha' = u\mathbf{E}f_{t-1} \quad (11)$$

$$\beta' = u(1 - \mathbf{E}f_{t-1}) \quad (12)$$

$$u \equiv \frac{\mathbf{E}f_{t-1}(1 - \mathbf{E}f_{t-1})}{\text{var } f_{t-1}} - 1. \quad (13)$$

155 The other components of the BMWS model are the “spikes” at $f_t = 0$ and $f_t = 1$. They are
156 handled similarly to the original BWS model: at each mating event $f_t \rightarrow f_{t-1}$, some amount
157 of probability mass is leaked from the beta (mixture) component to atomic components,
158 corresponding to the events $F_{t-1} = 0$ and $F_{t-1} = 2N_{t-1}$ in (2). (See the next section for a
159 precise statement.)

160 More generally, suppose the continuous component of f_t is a mixture, as in (7). We
 161 make the following approximation in order to cheaply compute the conditional density of
 162 f_{t-1} . Let C_t have the categorical distribution $\mathbf{P}(C_t = m) \propto c_{tm}$, $c \in \{0, \dots, M\}$, and
 163 interpret (7) hierarchically as

$$f_t | C_t = m \sim \text{Beta}(\alpha_{tm}, \beta_{tm}). \quad (14)$$

164 We assume that the continuous component of f_{t-1} is again a mixture of beta densities,
 165 with parameters $\alpha'_{tm}, \beta'_{tm}$ obtained by applying equations (11)–(13) with $\mathbf{E}(f_{t-1} | C_t = m)$
 166 (specified by equation 14) in place of $\mathbf{E}f_{t-1}$. That is, we separately compute the effect of
 167 (2) on each mixture component in (7), and average the results together using the mixing
 168 weights \mathbf{c}_t . This “linear” approximation requires only $\mathcal{O}(M)$ computations, and is much
 169 more efficient and easier to implement compared to modeling the effect of applying (2)
 170 to the overall mixture shown in (7). While a closer approximation could be obtained
 171 by optimizing over the mixture weights \mathbf{c}_t , it would introduce additional computational
 172 expense, and did not seem necessary in the examples we considered.

173 The astute reader will have noticed that, in contrast to some earlier works, we did not
 174 properly condition on non-fixation when constructing this approximation. That is, instead
 175 of e.g. $\mathbf{E}f_{t-1}$ in (8), we should instead have considered

$$\mathbf{E}(f_{t-1} | 0 < F_{t-1} < 2N_{t-1}).$$

176 However, the resulting expressions are very complex because they involve taking expectation
 177 over terms of the form $(f'_t)^k$ for k as high as $2N_{t-1}$. We opted for the simpler and more
 178 numerically stable equations (8)–(10), and confirmed in simulations that the model is still
 179 accurate across a range of parameter settings.

180 Likelihood

181 The likelihood (4) is calculated using a variant of the usual forward algorithm for hidden
 182 Markov models. We explain this computation in greater detail here since the approach is

183 nonstandard.

184 The forward algorithm recursively updates the so-called *filtering density* $p(f_t | a_t, \dots, a_T)$,
 185 which takes the form shown in equation (7) under our model. Given the filtering density
 186 and the observation a_{t-1} , we need to extend the filtering density one step towards the
 187 present to obtain $p(f_{t-1} | a_{t-1}, \dots, a_T)$. This is accomplished in stages:

188 1. We use equations (8)–(12) to compute α'_{tm} and β'_{tm} , as well as

$$p'_{t0} = p_{t0} + \mathbf{E} [p(F_{t-1} = 0 | f_t, a_t, \dots, a_T)]$$

189 and similarly for p'_{t1} . This yields the predictive density

$$p_s(f_{t-1} | a_t, \dots, a_T) = p'_{t0} \delta_0 + p'_{t1} \delta_1 + \sum_{m=0}^M c'_{tm} \text{Beta}(\alpha'_{tm}, \beta'_{tm}), \quad (15)$$

190 where we defined $c'_{tm} = (1 - p'_{t0} - p'_{t1}) c_{tm}$.

191 2. We compute the probability

$$p_s(a_{t-1} | a_t, \dots, a_T) = \int_{f_{t-1}} p(a_{t-1} | f_{t-1}) p_s(f_{t-1} | a_t, \dots, a_T),$$

192 noting that the integral can be evaluated analytically using equations (1) and (15),
 193 and conjugacy.

194 3. We update the mixture weights in (15) to incorporate the information added by
 195 observation a_{t-1} . Viewing a_{t-1} as a draw from the Bayesian hierarchical model defined
 196 by (1) and (15), the posterior mixture weights on the beta mixture components are

$$c_{t-1,m} | a_{t-1}, \dots, a_T \propto c'_{t,m} \binom{n_{t-1}}{a_{t-1}} \frac{\text{B}(a_{t-1} + \alpha'_{tm}, n_{t-1} - a_{t-1} + \beta'_{tm})}{\text{B}(\alpha'_{tm}, \beta'_{tm})}, \quad (16)$$

197 where the right-hand side is the $\text{BetaBinomial}(n_{t-1}, \alpha'_{tm}, \beta'_{tm})$ p.m.f. The posterior
 198 weight on the atom at $f_{t-1} = 1$ is $p_{t-1,1} \propto \mathbf{1}_{\{a_{t-1}=n_{t-1}\}}$, and similarly for $p_{t-1,0}$. The
 199 constant of proportionality in these equations is $p_s(a_{t-1} | a_t, \dots, a_T)$, calculated in
 200 step 2.

201 4. The filtering distribution $p_{\mathbf{s}}(f_{t-1} \mid a_{t-1}, \dots, a_T)$ takes the same form as (7), with
 202 mixture weights as defined in the preceding step, $\alpha_{t-1,m} = a_{t-1} + \alpha'_{t,m}$ and $\beta_{t-1,m} =$
 203 $n_{t-1} - a_{t-1} + \beta'_{t,m}$.

204 Recalling equation (4), the log-likelihood of the data is then

$$\log p_{\mathbf{s}}(\mathbf{a}) = \sum_{t=0}^T \log p_{\mathbf{s}}(a_t \mid a_{t+1}, \dots, a_T). \quad (17)$$

205 The running time of this algorithm is $\mathcal{O}(TM)$, as opposed to the standard forward algorithm
 206 which scales quadratically in M if it were to denote the number of hidden states in an HMM.
 207 This enables us to set M fairly large, ensuring that our model can flexibly approximate
 208 differently shaped filtering distributions.

209 Prior distribution

210 The filtering recursion is initialized by setting $p(f_T) = \pi_T(f_T)$, where π_T is a prior on the
 211 ancestral allele frequency. When developing our method, we observed that the choice of
 212 prior affected the accuracy of inferences in the ancient past when analysing aDNA data.
 213 This is because when the data are sparsely observed and allele counts are low, there is
 214 not enough data to overwhelm the prior in the early stages of the Markov chain. An
 215 uninformative choice of π_T can falsely suggest that the selected allele experienced a large
 216 change in frequency, potentially generating a spurious signal of selection. To mitigate this
 217 effect, we adopted a coordinate-ascent approach where we alternatively maximized the log-
 218 likelihood (17) with respect to a) the selective trajectory \mathbf{s} and b) the prior π_T .

219 For the prior distribution, we assumed that $\pi_T \sim \text{Beta}(\alpha_T, \beta_T)$ and optimized over
 220 α_T, β_T . Although this choice of prior is not necessarily in the family of $\text{Beta}(i+1, n-i+1)$
 221 mixture densities which comprise the interpolation scheme (6), we can accurately approxi-
 222 mate it (or any other choice of prior) by setting M large, setting $c_{Tm} \propto f_{\pi_T}(m/M)$, where
 223 f_{π_T} is the prior's density function, and invoking the aforementioned Bernstein approxima-
 224 tion theorem.

225 Inference

226 Given the probability model and approximations described in the preceding section, infer-
 227 ence is now straightforward. Parameter estimation is carried as described in the previous
 228 section, with one additional modification. Depending on the quality and density of the
 229 data, many entries of \mathbf{s} may only be weakly resolved, and we also found it advantageous to
 230 add a regularization term. The objective function for all the analyses reported below was

$$\max_{\mathbf{s}} \log p_{\mathbf{s}}(\mathbf{a}) - \lambda \sum_{t=0}^{T-1} (s_{t+1} - s_t)^2, \quad (18)$$

231 where $\lambda > 0$ is a tuning parameter. The regularizer penalizes variation in \mathbf{s} , with larger
 232 values of λ shrinking all entries towards a single common value, $s_0 = \dots = s_T$. The number
 233 of mixture components for the BMWS model was fixed to $M = 100$, and we performed
 234 three rounds of coordinate ascent. For all the examples in this paper, we assumed that the
 235 size history (N_0, \dots, N_T) is known, but co-estimation of selection and size history is also
 236 possible using our method, and could be an avenue for future research. Finally, our method
 237 is implemented using a JIT-compiled, differentiable programming language (Bradbury et al.,
 238 2018) to allow for efficient, gradient-based fitting.

239 We use a parametric bootstrap to estimate the uncertainty in our inference. Specifi-
 240 cally, after fitting the model, we sample allele frequency trajectories \mathbf{f} from the posterior
 241 distribution (equation 7). We then sample observations conditional on the trajectory and
 242 the original sample sizes and times, and refit the model to those observations. We repeat
 243 this 1000 times, and use the central 95% of results (based on the the mean value of \mathbf{s}) as
 244 an estimate of the 95% credible interval for \mathbf{s} , taking into account the uncertainty in the
 245 allele frequency trajectory, and the sampling of observations.

246 Simulations

247 We evaluated the performance of the estimator under three different types of selection, each
 248 lasting for $T = 100$ generations:

- 249 • Constant selection with $s = 0.01$ and initial frequency of 0.1.
- 250 • Selection that decreases sinusoidally from $s = +0.02$ to $s = -0.02$ and initial fre-
- 251 quency of 0.1.
- 252 • Selection that alternates between $+0.02$ and -0.02 every 20 generations and initial
- 253 frequency of 0.5.

254 In each case, we simulated allele frequency trajectories in a Wright-Fisher population with
255 $N = 10^4$ and then sampled 100 haploid individuals every 10 generations. We also simulated
256 the same selective models under two scenarios of variable effective population size:

- 257 • Exponential growth from $N = 10^4$ to $N = 10^5$.
- 258 • $N = 10^4$ with a bottleneck of $N = 10^3$ lasting 10 generations.

259 For these scenarios we ran the estimator both with the correct effective population size and
260 incorrectly assuming a constant $N = 10^4$ to evaluate its robustness to misspecification of
261 N . We varied the smoothing parameter λ from $\log_{10}(\lambda) = 1$ to 6 and report the root mean
262 squared (RMS) bias, variance and total error of the estimator. Finally, we evaluated the
263 error of the estimator as the sample size and frequency vary.

264 These simulations explore the effects of relatively strong selection with human-like demo-
265 graphic parameters ($N = 10^4$, 100 generations of observations, bottlenecks and exponential
266 growth, selection coefficients of $\mathcal{O}(0.01)$). However, other species may have very different
267 sets of parameters. We therefore recommend that for any particular application, users
268 should run simulations based on their prior parameter values in order to understand the
269 behavior of the estimator in their specific case, and to determine the appropriate smoothing
270 parameter. We provide functions to easily implement simulations under arbitrary selective
271 and population size scenarios. To illustrate this approach, we also ran the simulations de-
272 scribed above using the sampling distribution of the British aDNA data used in the rest of
273 paper.

274 Ancient DNA data

275 We collected data from ancient British individuals dated to the past 4500 years from the
276 Allen Ancient DNA resource ([Reich Lab, 2021](#)), and from original sources ([Schiffels et al.,](#)
277 [2016](#); [Martiniano et al., 2016](#); [Olalde et al., 2018](#); [Brace et al., 2019](#); [Margaryan et al., 2020](#);
278 [Patterson et al., 2022](#)). Most samples had been sequenced at sites targeted using the 1240k
279 in-solution capture reagent, and the small number of shotgun samples had been genotyped
280 at the 1240k SNPs so we therefore restricted our analysis to this set of SNPs. All data were
281 pseudo-haploid. After removing 22 PCA outliers, we were left with 529 ancient individuals
282 and 98 present-day individuals from the GBR population of the 1000 Genomes Project
283 ([The 1000 Genomes Project Consortium, 2015](#)), processed into pseudo-haploid data as part
284 of the AADR (Fig. 2A).

285 Our method assumes that samples are drawn from a closed, randomly mating popula-
286 tion in which every individual experiences the same selective pressures. While no natural
287 population satisfies these conditions, we chose to restrict to Britain dated in the period
288 4500BP-present because it is the largest aDNA sample from a time and region that comes
289 close to satisfying the assumptions of the model, for the following reasons. First, Britain is a
290 relatively small region (compared to previous Europe-wide studies), meaning that selective
291 pressures are more likely to be shared. Second, we know from previous aDNA studies that
292 the last major change in ancestry in Britain occurred around 4500BP ([Olalde et al., 2018](#)).
293 While recent work has demonstrated more recent Bronze Age migrations into Britain ([Pat-](#)
294 [terson et al., 2022](#)), these involved populations that were genetically similar, and inhabited
295 geographically adjacent regions. Third, we confirmed using principal component analysis
296 (PCA) that all the ancient samples in our analysis clustered with the present-day British
297 individuals from the 1000 Genomes project, and more broadly with other Northwestern
298 European individuals in the context of present-day West Eurasia (Fig. 2B).

299 Ancient DNA analysis

300 Starting with 1,150,639 autosomal SNPs, we removed 428,624 with a minor allele frequency
301 (MAF) < 0.1 in the full dataset on the grounds that any SNP with a significant frequency
302 shift in this time period would have intermediate MAF. We also removed 101,967 SNPs
303 with greater than 90% missingness and 210,725 SNPs with MAF=0 in the ancient data to
304 leave 409,232 SNPs genome-wide. We inferred selection coefficients \hat{s}_t at generation t for
305 every SNP in the filtered data using a smoothing parameter of $\lambda = 10^{4.5}$ and an effective
306 population size of $N = 10^4$. For each SNP, we summarize this estimate by the mean
307 selection coefficient $\bar{s} = \frac{1}{T} \sum_{t=1}^T \hat{s}_t$, and the root mean squared selection coefficient $\|s\| =$
308 $\left(T^{-1} \sum_{t=1}^T \hat{s}_t^2\right)^{1/2}$. We then computed the mean value of $\|s\|$ in 20-SNP sliding windows,
309 sliding in 10 SNP increments, so each SNP contributes to two windows. We denote these
310 window statistics $\|s\|_{20}$. Finally, we fit a gamma distribution using the method of moments
311 to the values of $\|s\|_{20}$, and used this fitted distribution to compute P-values for each window.
312 We therefore calibrate the test statistics to the genome-wide background, analogous to the
313 use of Genomic Control to account for genetic drift in association studies. We confirmed
314 that this procedure leads to well-calibrated P-values when there is no temporal change in
315 allele frequencies by repeating the analysis with the dates of each sample randomized.

316 We compared our results with two previous genome-wide selection scans. The first—an
317 aDNA based scan (Mathieson et al., 2015)—is an allele frequency scan to detect selection
318 in approximately the last 8,000 years in Western Eurasia. The second, the SDS test (Field
319 et al., 2016), is a scan based on haplotype lengths in the present-day UK population and is
320 most sensitive to selection in the past few thousand years. First, we restricted the previous
321 scans to the same set of SNPs used in the present scan. Next, for each window in the present
322 scan, we computed the mean test statistics (chi-squared statistic for the aDNA scan and
323 squared Z -score for the SDS) in each window and compared to the test statistics generated
324 by our method.

325 Polygenic selection test

326 We obtained summary statistics from genome-wide association studies (GWAS) for 28 quan-
327 titative traits (Neale Lab, 2021; Taal et al., 2012; Wood et al., 2014; Horikoshi et al., 2016;
328 Chen et al., 2021). We took the intersection of GWAS SNPs with the 1240k SNPs, restricted
329 to P-values $< 10^{-4}$, and pruned to an independent set of SNPs by iteratively taking the
330 SNP with the smallest P-value and removing all other SNPs within 250kb. For each trait,
331 we calculated the correlation between effect size and estimated selection coefficient for each
332 independent SNP.

333 Results

334 Our estimator successfully recovers complex selection trajectories from simulated data
335 (Fig. 3), with total sample sizes and times equal to the ancient sample, though individual se-
336 lection coefficient estimates can have considerable uncertainty—on the order of $\pm 0.01 - 0.02$
337 with these parameter values. This suggests that with the data available we should be able
338 to reliably detect selection coefficients around 0.02, similar to the SDS and aDNA allele
339 frequency approaches that we compare with (Mathieson et al., 2015; Field et al., 2016).
340 The absolute error of the estimate does not depend on the selection coefficient, meaning
341 that, at least in this parameter range, we cannot reliably distinguish smaller selection co-
342 efficients from zero. As expected, the optimal smoothing parameter depends on the true
343 selective trajectory—the smoother the trajectory, the higher the optimal λ (Supplemental
344 Fig. S1). We therefore recommend choosing λ based on simulations, with parameters that
345 are informed by the specific application.

346 The estimator performs similarly in the presence of population size bottlenecks or ex-
347 ponential growth, although it tends to slightly over-smooth changes in s in these cases
348 (Supplemental Fig. S2). It is relatively robust to mis-specification of effective population
349 size: if we input constant N to the estimator, results are not noticeably different than if

350 we specify the correct population size history (Supplemental Fig. S3). Increasing size and
351 frequency of sampling reduces error (Supplemental Fig. S4) though, in general, sample size
352 is more important than sampling frequency and, all else being equal, it is better to have
353 infrequent samples of large sizes than frequent small samples.

354 In the ancient British data, we identified 7 regions with genome-wide significant evidence
355 of selection (Table 1, Fig. 4A, supplemental Table S2). We used a P-value cutoff of 10^{-7}
356 as a genome-wide significant cutoff. While conservative for the 68,061 overlapping windows
357 in our analysis, we used this value because when we reran the analysis with randomized
358 sample dates, no window had a smaller P-value (Fig. 4B). Three of these regions, which we
359 denote HLA1, HLA2, and HLA3 are in the HLA region on Chromosome 6 (Supplemental
360 Fig. S5), though these themselves may contain multiple signals. An eighth apparent signal
361 on Chromosome 4 containing the gene *LINC00955* is likely artefactual. The lead SNP
362 rs4690044 has a MAF of 0 in present-day samples but around 0.5 in ancient samples. In
363 gnomAD (Karczewski et al., 2020), rs4690044 has a MAF of 0.48, but no homozygotes,
364 suggesting an artefactual call caused by a duplication. An additional locus on Chromosome
365 12 ($P=2.5 \times 10^{-7}$) which contains the gene *OAS1* and is known to be a target of adaptive
366 Neanderthal introgression (Sams et al., 2016) was significant at a Bonferroni corrected
367 significance threshold ($P=7.3 \times 10^{-7}$).

368 All seven of these regions were identified by a previous allele frequency based selection
369 scan using aDNA to detect selection in West Eurasia over the past 8,000 years (Mathieson
370 et al., 2015) (Fig. 4D). Only *LCT* and the HLA region show significant evidence of selection
371 in a haplotype-based scan using present-day sequence data that aimed to detect selection
372 in Britain in the past few thousand years (Field et al., 2016) (Fig. 4C) or in a scan based on
373 identifying very recent coalescence times (~ 50 generations) in the UK Biobank (Nait Saada
374 et al., 2020).

375 For the non-HLA signals where we have a strong candidate for the causal variant based
376 on previous literature, we examined the precise timing and trajectory of selection estimates

Locus	Chr	Start (hg19)	End (hg19)	Target SNP	Allele	\bar{s}
<i>LCT</i>	2	136,582,694	136,714,178	rs4988235	G	0.064
<i>SLC45A2</i>	5	33,887,419	33,964,938	rs16891982	C	0.043
HLA1	6	28,234,597	28,374,902	(rs6922111)	(C)	(0.046)
HLA2	6	31,026,009	31,361,897	(rs4947296)	(C)	(0.034)
HLA3	6	32,083,175	32,581,973	(rs204994)	(C)	(0.042)
<i>DHCR7</i>	11	71,142,350	71,183,690	rs7944926	A	0.051
<i>HERC2</i>	15	28,334,927	28,526,228	rs12913832	A	0.017

Table 1: Genome-wide significant regions. For non-HLA regions, we give the chromosome and position of the center of the lead window, the selected SNP (based on previous literature), the selected allele, and the mean selection coefficient of the lead SNP. For HLA regions we give the co-ordinates of the three regions that contain significant signals (Supplemental Fig. S5), and the SNPs with the largest test statistic $\|s\|$. Parentheses indicate that we do not know whether these specific SNPs were the targets of selection. \bar{s} is the average selection coefficient over the observed time period.

377 from our model (Fig. 5). The most significant signal was the well-known *LCT* locus on
378 Chromosome 2, where the selected allele is associated with lactase persistence (Enattah
379 et al., 2002; Bersaglieri et al., 2004). We find that selection for the persistence allele was
380 strongest ($s \approx 0.08$) from 150 to 100 generations before present (roughly 4500 – 3000BP)
381 before decreasing to around 0.02 in the past 50 generations. This large change in strength
382 of selection might explain the wide range of estimates from models that assume a constant
383 value (Mathieson and Mathieson, 2018; Bersaglieri et al., 2004; Peter et al., 2012). At
384 *DHCR7*, the haplotype tagged by the SNP in our analysis, rs7944926, is associated with
385 protection against vitamin D insufficiency (Wang et al., 2010) and has been shown to have
386 been under recent selection in both Europe (Mathieson et al., 2015) and East Asia (Kuan
387 et al., 2013). We infer that, in Britain, the selection coefficient increased over the past 150

388 generations, from around 0 to 0.06, leading to an increase in frequency from about 20% to
389 60% over the past 3000 years (Fig. 5).

390 Derived alleles at *SLC45A2* and *HERC2* are associated with light skin, hair and eye
391 pigmentation (Norton et al., 2007; Eiberg et al., 2008; Canela-Xandri et al., 2018; Hysi
392 et al., 2018; Simcoe et al., 2021). Both these alleles have been shown to have been under
393 selection broadly in Europe (Norton et al., 2007; Lao et al., 2007; Donnelly et al., 2012)
394 and specifically during the Holocene (Wilde et al., 2014; Mathieson et al., 2015). Time
395 series of aDNA have shown that both alleles were under selection in the past 5000 years
396 in Eastern Europe (Wilde et al., 2014). There, the derived *SLC45A2* allele increased in
397 frequency from 40% to 90% over the past 5000 years, suggesting a selection coefficient
398 of around 0.03, very similar to our estimate of selection in Britain during the same time
399 (Fig. 5). For the derived *HERC2* allele, we estimate a selection coefficient of 0.02-0.04,
400 similar to that estimated in Eastern Europe, although we find that in Britain selection was
401 largely restricted to approximately the past 2000 years. Wilde et al. (2014) also found a
402 derived allele of *TYR* to be under strong selection in Eastern Europe, but we find little
403 evidence that it was under selection in Britain, except possibly before 3000BP (window
404 P-value=0.03, Supplemental Fig. S6).

405 At the HLA we find three regions with genome-wide significant evidence of selection,
406 which we denote HLA1-3 (Fig. S5). All three correspond to regions identified by Mathieson
407 et al. (2015) and also have strong evidence of selection in the Field et al. (2016) scan
408 (Fig. 4C). Because of high gene density and complex patterns of linkage disequilibrium in
409 the region, we did not attempt to identify causal genes or variants. However we note that
410 the lead SNP at HLA1 is strongly associated with decreased risk of coeliac disease in UK
411 Biobank (Canela-Xandri et al., 2018). The lead HLA2 SNP is associated with increased
412 risk of ankylosing spondylitis (Canela-Xandri et al., 2018) but the region contains the gene
413 *HLA-C*, a variant of which is the strongest known risk factor for psoriasis (Yin et al., 2015).
414 Finally, the lead SNP at HLA3 is strongly associated with decreased risk of coeliac disease

415 and psoriasis ([Canela-Xandri et al., 2018](#)). These associations suggest that risk of these
416 diseases has been affected by selection, even if they themselves are not the direct targets.

417 Finally, we searched for evidence of polygenic selection by testing for a correlation
418 between GWAS effect size and selection coefficient for 28 anthropometric and morphological
419 traits (Fig. 6A, Table S1, Supplemental Fig. S7). We find significant evidence of polygenic
420 selection for reduced skin pigmentation ($P=3.6 \times 10^{-16}$, Fig. 6B) but none of the other 27
421 traits ($P > 0.04$). Though not statistically significant, the largest absolute correlation apart
422 from skin pigmentation is for increased calcium. We do not detect evidence of selection on
423 any of the phenotypes identified by [Field et al. \(2016\)](#) as under selection in Britain in the
424 past 2000 years, including height, infant head circumference and fasting insulin.

425 Discussion

426 Our fast and flexible estimator allowed us to perform a direct genome-wide scan for selection
427 based on allele frequency trajectories. On our standard compute cluster, average run-time
428 for each SNP was 41s, requiring 220Mb of RAM, so analyzing all 1240k loci took around
429 13,000 CPU-hours in total. All of the significant loci we identified have been identified
430 by a previous allele frequency based scan using aDNA ([Mathieson et al., 2015](#)). However,
431 that approach scanned for selection broadly in Holocene Europe and was unable to localize
432 selection further in either space or time. Here, we are able to localize selection to Britain in
433 the past 4500 years and, even further, to identify changes in the strength of selection over
434 that time period (Fig. 5). We are also able to identify selected loci that were not identified
435 in studies of much larger samples of present-day individuals ([Field et al., 2016](#); [Nait Saada
436 et al., 2020](#)).

437 On the other hand, when we search for polygenic selection, the only trait for which we
438 find significant evidence is skin pigmentation, which is known to have been under selection
439 in Europe more broadly into this time period ([Wilde et al., 2014](#); [Mathieson et al., 2015](#);
440 [Field et al., 2016](#); [Ju and Mathieson, 2021](#)). Though many previous studies ([Turchin et al.,](#)

441 2012; Berg and Coop, 2014; Robinson et al., 2015; Mathieson et al., 2015; Field et al., 2016)
442 reported evidence for recent selection on height, this has been shown to be largely driven
443 by residual stratification in the GIANT consortium GWAS (Berg et al., 2019; Sohail et al.,
444 2019). Evidence of recent polygenic selection for other traits (e.g., Field et al., 2016) may
445 suffer from the same issue, although findings based on UK Biobank GWAS results may be
446 more reliable. It is also possible that our negative findings reflect a lack of power. Even
447 though our approach is relatively well-powered to detect strong selection compared to other
448 selection scans, it may be less able to detect the weak selection that contributes to polygenic
449 adaptation even in aggregate. A more complete investigation of the way in which the time
450 series analysis in this study could be used to detect polygenic selection is a question for
451 future work.

452 While there may have been multiple environmental drivers of selection, taken together
453 our results strongly suggest that a major selective pressure at this time was for increased
454 calcium largely moderated through increased vitamin D levels. Vitamin D is required for
455 the absorption of calcium and deficiency leads to bone deformities with potentially major
456 effects on fitness. Since a major source of vitamin D is synthesis in the skin in the presence
457 of UV radiation, the cloudy skies of Britain are likely to have limited this synthesis. The
458 Mesolithic inhabitants of Britain may have avoided this problem through consumption of
459 vitamin D rich marine resources, but later Neolithic and Bronze Age populations including
460 those in our study relied on agricultural products for their subsistence (Richards et al.,
461 2003), leading to a need for genetic adaptation.

462 In fact, almost all of our signals of selection can be related to selection for increased
463 vitamin D or directly for increased calcium. Selection at *SLC45A2* and *HERC2*, and selec-
464 tion for lighter skin pigmentation more generally, naturally lead to increased penetration
465 of UV into the skin and therefore higher levels of vitamin D (Murray, 1934; Jablonski and
466 Chaplin, 2010). Lactase persistence allows the consumption of milk which contains both
467 calcium and a small amount of vitamin D. This “calcium absorption” hypothesis has long

468 been suggested to explain the high frequency of the persistence phenotype in Northern Eu-
469 rope (Flatz and Rotthauwe, 1973; Gerbault et al., 2011). *DHCR7* is directly involved in
470 vitamin D metabolism and the selected allele protects against insufficiency (Wang et al.,
471 2010). While the HLA associations are more difficult to specifically identify, two of the
472 selected alleles are protective against coeliac disease which itself is a risk factor for mal-
473 absorption of calcium and vitamin D, and consequent osteoporosis (Meyer et al., 2001).
474 Strong selective pressure for increased vitamin D and calcium levels is therefore a plausible
475 and parsimonious explanation for the patterns of selection that we observe in this dataset.

476 The main limitation of our approach is the assumption of population continuity. Al-
477 though there is evidence of external migration into Britain during the time period we
478 investigated (Patterson et al., 2022), there is relatively little change in genetic ancestry
479 since the sources of that migration are genetically similar populations from other nearby
480 parts of Northern Europe. If this affects our results it would likely mean that some of the
481 selection we detected actually occurred in those neighboring populations, somewhat earlier
482 than the dates we find here. However, given that the selection pressures we detect are
483 likely to be shared with these similar populations anyway, we do not think this possibility
484 has a major impact on the interpretation of our results. This limitation is more serious if
485 we want to extend the temporal and geographic range of our analysis. In particular, both
486 ancient and present-day individuals from the Iberian and Italian peninsulas are much more
487 genetically diverse than those from Britain (Supplemental Fig. S8). Because of this, and the
488 much smaller ancient sample sizes, we did not analyze selection in these Southern European
489 populations, although identifying differences in selective pressures between Northern and
490 Southern Europe is an important direction for future analysis.

491 Although we have identified the loci under the strongest selection in recent British
492 history, there is evidence in our data of additional selected loci. For example, several
493 known loci including *OAS1* ($P=2.5 \times 10^{-7}$, Sams et al. (2016)) and *FADS1* ($P=1.5 \times 10^{-5}$,
494 Mathieson et al. (2015)) have evidence of selection though below genome-wide significance.

495 With larger sample sizes we can expect that these and other, potentially novel, loci would
496 be identified. An alternative way to increase sample size would be to modify our method to
497 analyze genotype likelihoods rather than pseudohaploid calls. We estimate that this could
498 increase effective sample size by up to 22%. An even bigger increase could be gained by
499 using genotype imputation although with the caveat that imputation may be less reliable
500 in strongly selected regions. There are also several technical limitations that may affect
501 interpretations of our results. For example, we identified at least one locus where systematic
502 differences between ancient and present-day samples created a spurious signal of selection.
503 Other systematic differences related to mapping errors, or ancient DNA damage, might
504 create similar effects. It is important therefore to check that results based on comparison
505 of ancient and present-day samples are robust by verifying that they are consistent when
506 present-day samples are excluded or, as we have done here, that they are consistent with
507 signals derived from present-day data alone. Another limitation is that we rely on sites
508 included in the 1240k capture reagent, and therefore cannot detect selection on rare SNPs
509 or structural variants that are not tagged by such SNPs. Imputation or large datasets
510 of shotgun sequence data might extend the range of variation on which selection can be
511 detected.

512 Our study demonstrates the power of ancient DNA to robustly detect and precisely
513 characterize the timing of natural selection in humans. We appear to have similar power to
514 detect selection as previously published methods based on present-day and ancient data. On
515 the other hand, present-day sample sizes will always be much larger and approaches that can
516 scale to hundreds of thousands or millions of genomes (Nait Saada et al., 2020) will probably
517 be more powerful. The major advantage of ancient DNA is the ability to precisely estimate
518 the timing of selection, suggesting a potential hybrid approach using very large present-day
519 datasets to identify non-neutral regions of the genome and then use ancient DNA time series
520 to characterize the timing and nature of selection at those loci. Indeed, several of the loci
521 that we identify have evidence of substantial change in the strength of selection over the

522 past 4500 years, suggesting that modeling this variability may be an important addition to
523 previous approaches that assume constant selective pressure. One caveat is that in order to
524 do this, we need to be able to identify the selected variant at a locus, which is not always
525 possible (for example in the case of HLA). Indeed, imperfect tagging of the causal variant
526 could lead to spurious signals of time-varying selection, as could dominance coefficients
527 different from 0.5 or spatially structured selection. In particular, lactase persistence is
528 dominant, though enzymatic activity is not (Segurel and Bon, 2017). Therefore selection
529 on *LCT* could act in a dominant fashion, which could give the appearance of decreasing
530 selective coefficient over time. If the selective pressure on *LCT* did decrease over time,
531 perhaps due to cultural changes, it may have contributed to an increase in selective pressures
532 related to other sources (e.g., pigmentation and metabolism). In this way, culture could
533 have determined the genetic response to a constant environmental selective pressure. The
534 prospect of exploring this and similar interactions is an exciting future direction for ancient
535 DNA research.

536 **Software availability**

537 Code to run the estimator and reproduce the analyses in this paper is included as Supple-
538 mental Code S3 and also available at <https://github.com/jthlab/bmws>.

539 **Competing interest statement**

540 The authors declare no competing interests.

541 **Acknowledgments**

542 We thank Pontus Skoglund for helpful comments. This research was funded by the NIGMS
543 ([R35GM133708] to I.M.) and the NSF ([DMS-2052653] to J.T.). The content is solely

544 the responsibility of the authors and does not necessarily represent the official views of the
545 funding agencies.

546

547 *Author contributions:* I.M. and J.T. conceived and designed the study, wrote code, analyzed
548 data and wrote the manuscript.

549 References

550 Berg, J. J. and Coop, G., 2014. A population genetic signal of polygenic adaptation. *PLoS*
551 *Genet*, **10**(8):e1004412.

552 Berg, J. J., Harpak, A., Sinnott-Armstrong, N., Joergensen, A. M., Mostafavi, H., Field,
553 Y., Boyle, E. A., Zhang, X., Racimo, F., Pritchard, J. K., *et al.*, 2019. Reduced signal
554 for polygenic adaptation of height in uk biobank. *Elife*, **8**:e39725.

555 Bersaglieri, T., Sabeti, P. C., Patterson, N., Vanderploeg, T., Schaffner, S. F., Drake, J. A.,
556 Rhodes, M., Reich, D. E., and Hirschhorn, J. N., 2004. Genetic signatures of strong
557 recent positive selection at the lactase gene. *Am J Hum Genet*, **74**(6):1111–20.

558 Bollback, J. P., York, T. L., and Nielsen, R., 2008. Estimation of $2n\mu$ from temporal allele
559 frequency data. *Genetics*, **179**(1):497–502.

560 Brace, S., Diekmann, Y., Booth, T. J., van Dorp, L., Faltyskova, Z., Rohland, N., Mallick,
561 S., Olalde, I., Ferry, M., Michel, M., *et al.*, 2019. Ancient genomes indicate population
562 replacement in early neolithic britain. *Nat Ecol Evol*, **3**(5):765–771.

563 Bradbury, J., Frostig, R., Hawkins, P., Johnson, M. J., Leary, C., Maclaurin, D., Necula,
564 G., Paszke, A., VanderPlas, J., Wanderman-Milne, S., *et al.*, 2018. JAX: composable
565 transformations of Python+NumPy programs.

566 Canela-Xandri, O., Rawlik, K., and Tenesa, A., 2018. An atlas of genetic associations in
567 uk biobank. *Nat Genet*, **50**(11):1593–1599.

- 568 Chen, J., Spracklen, C. N., Marenne, G., Varshney, A., Corbin, L. J., Luan, J., Willems,
569 S. M., Wu, Y., Zhang, X., Horikoshi, M., *et al.*, 2021. The trans-ancestral genomic
570 architecture of glycemc traits. *Nat Genet*, **53**(6):840–860.
- 571 Donnelly, M. P., Paschou, P., Grigorenko, E., Gurwitz, D., Barta, C., Lu, R. B., Zhukova,
572 O. V., Kim, J. J., Siniscalco, M., New, M., *et al.*, 2012. A global view of the oca2-herc2
573 region and pigmentation. *Hum Genet*, **131**(5):683–96.
- 574 Eiberg, H., Troelsen, J., Nielsen, M., Mikkelsen, A., Mengel-From, J., Kjaer, K. W., and
575 Hansen, L., 2008. Blue eye color in humans may be caused by a perfectly associated
576 founder mutation in a regulatory element located within the herc2 gene inhibiting oca2
577 expression. *Hum Genet*, **123**(2):177–87.
- 578 Enattah, N. S., Sahi, T., Savilahti, E., Terwilliger, J. D., Peltonen, L., and Jarvela, I.,
579 2002. Identification of a variant associated with adult-type hypolactasia. *Nat Genet*,
580 **30**(2):233–7.
- 581 Ewens, W. J., 2004. *Mathematical population genetics: theoretical introduction*, volume 1.
582 Springer.
- 583 Feder, A. F., Kryazhimskiy, S., and Plotkin, J. B., 2014. Identifying signatures of selection
584 in genetic time series. *Genetics*, **196**(2):509–522.
- 585 Feller, W., 2008. *An introduction to probability theory and its applications, vol 2*. John
586 Wiley & Sons.
- 587 Ferrer-Admetlla, A., Leuenberger, C., Jensen, J. D., and Wegmann, D., 2016. An approxi-
588 mate markov model for the wright–fisher diffusion and its application to time series data.
589 *Genetics*, **203**(2):831–846.
- 590 Field, Y., Boyle, E. A., Telis, N., Gao, Z., Gaulton, K. J., Golan, D., Yengo, L., Rocheleau,

- 591 G., Froguel, P., McCarthy, M. I., *et al.*, 2016. Detection of human adaptation during the
592 past 2000 years. *Science*, **354**(6313):760–764.
- 593 Flatz, G. and Rotthauwe, H. W., 1973. Lactose nutrition and natural selection. *Lancet*,
594 **2**(7820):76–7.
- 595 Gerbault, P., Liebert, A., Itan, Y., Powell, A., Currat, M., Burger, J., Swallow, D. M.,
596 and Thomas, M. G., 2011. Evolution of lactase persistence: an example of human niche
597 construction. *Philos Trans R Soc Lond B Biol Sci*, **366**(1566):863–77.
- 598 Gompert, Z., 2016. Bayesian inference of selection in a heterogeneous environment from
599 genetic time-series data. *Mol. Ecol.*, **1**.
- 600 Horikoshi, M., Beaumont, R. N., Day, F. R., Warrington, N. M., Kooijman, M. N.,
601 Fernandez-Tajes, J., Feenstra, B., van Zuydam, N. R., Gaulton, K. J., Grarup, N., *et al.*,
602 2016. Genome-wide associations for birth weight and correlations with adult disease.
603 *Nature*, **538**(7624):248–252.
- 604 Hysi, P. G., Valdes, A. M., Liu, F., Furlotte, N. A., Evans, D. M., Bataille, V., Visconti,
605 A., Hemani, G., McMahon, G., Ring, S. M., *et al.*, 2018. Genome-wide association meta-
606 analysis of individuals of european ancestry identifies new loci explaining a substantial
607 fraction of hair color variation and heritability. *Nat Genet*, **50**(5):652–656.
- 608 Jablonski, N. G. and Chaplin, G., 2010. Human skin pigmentation as an adaptation to uv
609 radiation. *Proc Natl Acad Sci U S A*, **107 Suppl 2**:8962–8.
- 610 Ju, D. and Mathieson, I., 2021. The evolution of skin pigmentation-associated variation in
611 west eurasia. *Proc Natl Acad Sci U S A*, **118**(1):e2009227118.
- 612 Karczewski, K. J., Francioli, L. C., Tiao, G., Cummings, B. B., Alfoldi, J., Wang, Q.,
613 Collins, R. L., Laricchia, K. M., Ganna, A., Birnbaum, D. P., *et al.*, 2020. The mutational

- 614 constraint spectrum quantified from variation in 141,456 humans. *Nature*, **581**(7809):434–
615 443.
- 616 Kerner, G., Laval, G., Patin, E., Boisson-Dupuis, S., Abel, L., Casanova, J. L., and
617 Quintana-Murci, L., 2021. Human ancient dna analyses reveal the high burden of tuber-
618 culosis in europeans over the last 2,000 years. *Am J Hum Genet*, **108**(3):517–524.
- 619 Kuan, V., Martineau, A. R., Griffiths, C. J., Hypponen, E., and Walton, R., 2013. Dhcr7
620 mutations linked to higher vitamin d status allowed early human migration to northern
621 latitudes. *BMC Evol Biol*, **13**:144.
- 622 Lacerda, M. and Seoighe, C., 2014. Population genetics inference for longitudinally-sampled
623 mutants under strong selection. *Genetics*, **198**(3):1237–1250.
- 624 Lao, O., de Gruijter, J. M., van Duijn, K., Navarro, A., and Kayser, M., 2007. Signatures
625 of positive selection in genes associated with human skin pigmentation as revealed from
626 analyses of single nucleotide polymorphisms. *Ann Hum Genet*, **71**(Pt 3):354–69.
- 627 Lazaridis, I., Patterson, N., Mittnik, A., Renaud, G., Mallick, S., Kirsanow, K., Sudmant,
628 P. H., Schraiber, J. G., Castellano, S., Lipson, M., *et al.*, 2014. Ancient human genomes
629 suggest three ancestral populations for present-day europeans. *Nature*, **513**(7518):409–13.
- 630 Malaspinas, A.-S., 2016. Methods to characterize selective sweeps using time serial samples:
631 an ancient DNA perspective. *Mol. Ecol.*, **25**(1):24–41.
- 632 Malaspinas, A.-S., Malaspinas, O., Evans, S. N., and Slatkin, M., 2012. Estimating allele
633 age and selection coefficient from time-serial data. *Genetics*, **192**(2):599–607.
- 634 Margaryan, A., Lawson, D. J., Sikora, M., Racimo, F., Rasmussen, S., Moltke, I., Cassidy,
635 L. M., Jorsboe, E., Ingason, A., Pedersen, M. W., *et al.*, 2020. Population genomics of
636 the viking world. *Nature*, **585**(7825):390–396.

- 637 Martiniano, R., Caffell, A., Holst, M., Hunter-Mann, K., Montgomery, J., Müldner, G.,
638 McLaughlin, R. L., Teasdale, M. D., Van Rhee, W., and Veldink, J. H., *et al.*, 2016.
639 Genomic signals of migration and continuity in Britain before the Anglo-Saxons. *Nature*
640 *communications*, **7**:10326.
- 641 Mathieson, I., Lazaridis, I., Rohland, N., Mallick, S., Patterson, N., Roodenberg, S. A., Har-
642 ney, E., Stewardson, K., Fernandes, D., Novak, M., *et al.*, 2015. Genome-wide patterns
643 of selection in 230 ancient Eurasians. *Nature*, **528**(7583):499–503.
- 644 Mathieson, I. and McVean, G., 2013. Estimating selection coefficients in spatially structured
645 populations from time series data of allele frequencies. *Genetics*, **193**(3):973–84.
- 646 Mathieson, S. and Mathieson, I., 2018. *FADS1* and the timing of human adaptation to
647 agriculture. *Mol Biol Evol*, **35**(12):2957–2970.
- 648 Meyer, D., Stavropoulos, S., Diamond, B., Shane, E., and Green, P. H., 2001. Osteoporosis
649 in a North American adult population with celiac disease. *Am J Gastroenterol*, **96**(1):112–
650 9.
- 651 Murray, F. G., 1934. Pigmentation, sunlight, and nutritional disease. *American Anthropol-*
652 *ogist*, **36**(3):438–445.
- 653 Nait Saada, J., Kalantzis, G., Shyr, D., Cooper, F., Robinson, M., Gusev, A., and Palamara,
654 P. F., 2020. Identity-by-descent detection across 487,409 British samples reveals fine scale
655 population structure and ultra-rare variant associations. *Nat Commun*, **11**(1):6130.
- 656 Neale Lab, 2021. UK Biobank GWAS Results. <http://www.nealelab.is/uk-biobank>. Ac-
657 cessed: 2021-01-20.
- 658 Norton, H. L., Kittles, R. A., Parra, E., McKeigue, P., Mao, X., Cheng, K., Canfield,
659 V. A., Bradley, D. G., McEvoy, B., and Shriver, M. D., *et al.*, 2007. Genetic evidence

- 660 for the convergent evolution of light skin in europeans and east asians. *Mol Biol Evol*,
661 24(3):710–22.
- 662 Olalde, I., Brace, S., Allentoft, M. E., Armit, I., Kristiansen, K., Booth, T., Rohland, N.,
663 Mallick, S., Szecsenyi-Nagy, A., Mittnik, A., *et al.*, 2018. The beaker phenomenon and
664 the genomic transformation of northwest europe. *Nature*, 555(7695):190–196.
- 665 Olalde, I., Mallick, S., Patterson, N., Rohland, N., Villalba-Mouco, V., Silva, M., Duijals,
666 K., Edwards, C. J., Gandini, F., Pala, M., *et al.*, 2019. The genomic history of the iberian
667 peninsula over the past 8000 years. *Science*, 363(6432):1230–1234.
- 668 Paris, C., Servin, B., and Boitard, S., 2019. Inference of selection from genetic time se-
669 ries using various parametric approximations to the wright-fisher model. *G3: Genes*,
670 *Genomes, Genetics*, 9(12):4073–4086.
- 671 Patterson, N., Isakov, M., Booth, T., Bustar, L., Fischer, C. E., Olalde, I., Ringbauer, H.,
672 Akbari, A., Cheronet, O., Bleasdale, M., *et al.*, 2022. Large-scale migration into britain
673 during the middle to late bronze age. *Nature*, 601(7894):588–594.
- 674 Peter, B. M., Huerta-Sanchez, E., and Nielsen, R., 2012. Distinguishing between se-
675 lective sweeps from standing variation and from a de novo mutation. *PLoS Genet*,
676 8(10):e1003011.
- 677 Reich Lab, 2021. Allen Ancient DNA Resource. <https://reich.hms.harvard.edu/allen-ancient-dna-resource-aadr-downloadable-genotypes-present-day-and-ancient-dna-data>.
678
679 Accessed: 2021-09-01.
- 680 Richards, M. P., Schulting, R. J., and Hedges, R. E., 2003. Archaeology: sharp shift in diet
681 at onset of neolithic. *Nature*, 425(6956):366.
- 682 Robinson, M. R., Hemani, G., Medina-Gomez, C., Mezzavilla, M., Esko, T., Shakhbazov,
683 K., Powell, J. E., Vinkhuyzen, A., Berndt, S. I., Gustafsson, S., *et al.*, 2015. Popula-

- 684 tion genetic differentiation of height and body mass index across europe. *Nat Genet*,
685 47(11):1357–62.
- 686 Sams, A. J., Dumaine, A., Nedelec, Y., Yotova, V., Alfieri, C., Tanner, J. E., Messer, P. W.,
687 and Barreiro, L. B., 2016. Adaptively introgressed neandertal haplotype at the oas locus
688 functionally impacts innate immune responses in humans. *Genome Biol*, 17(1):246.
- 689 Schiffels, S., Haak, W., Pajajanen, P., Llamas, B., Popescu, E., Loe, L., Clarke, R., Lyons,
690 A., Mortimer, R., and Sayer, D., *et al.*, 2016. Iron age and anglo-saxon genomes from
691 east england reveal british migration history. *Nature communications*, 7:10408.
- 692 Segurel, L. and Bon, C., 2017. On the evolution of lactase persistence in humans. *Annu*
693 *Rev Genomics Hum Genet*, 18:297–319.
- 694 Simcoe, M., Valdes, A., Liu, F., Furlotte, N. A., Evans, D. M., Hemani, G., Ring, S. M.,
695 Smith, G. D., Duffy, D. L., Zhu, G., *et al.*, 2021. Genome-wide association study in
696 almost 195,000 individuals identifies 50 previously unidentified genetic loci for eye color.
697 *Sci Adv*, 7(11):10.1126/sciadv.abd1239.
- 698 Skoglund, P. and Mathieson, I., 2018. Ancient genomics of modern humans: The first
699 decade. *Annu Rev Genomics Hum Genet*, 19:381–404.
- 700 Skoglund, P., Thompson, J. C., Prendergast, M. E., Mittnik, A., Sirak, K., Hajdinjak, M.,
701 Salie, T., Rohland, N., Mallick, S., Peltzer, A., *et al.*, 2017. Reconstructing prehistoric
702 african population structure. *Cell*, 171(1):59–71 e21.
- 703 Sohail, M., Maier, R. M., Ganna, A., Bloemendal, A., Martin, A. R., Turchin, M. C., Chi-
704 ang, C. W., Hirschhorn, J., Daly, M. J., Patterson, N., *et al.*, 2019. Polygenic adaptation
705 on height is overestimated due to uncorrected stratification in genome-wide association
706 studies. *Elife*, 8:e39702.

- 707 Steinrücken, M., Bhaskar, A., and Song, Y. S., 2014. A novel spectral method for inferring
708 general diploid selection from time series genetic data. *Ann. Appl. Stat.*, **8**(4):2203–2222.
- 709 Taal, H. R., Pourcain, B. S., Thiering, E., Das, S., Mook-Kanamori, D. O., Warrington,
710 N. M., Kaakinen, M., Kreiner-Moller, E., Bradfield, J. P., Freathy, R. M., *et al.*, 2012.
711 Common variants at 12q15 and 12q24 are associated with infant head circumference. *Nat*
712 *Genet*, **44**(5):532–538.
- 713 Tataru, P., Bataillon, T., and Hobolth, A., 2015. Inference under a Wright-Fisher model
714 using an accurate beta approximation. *Genetics*, **201**(3):1133–1141.
- 715 Tataru, P., Simonsen, M., Bataillon, T., and Hobolth, A., 2017. Statistical inference in the
716 Wright-Fisher model using allele frequency data. *Syst. Biol.*, **66**(1):e30–e46.
- 717 Terhorst, J., Schlötterer, C., and Song, Y. S., 2015. Multi-locus analysis of genomic time
718 series data from experimental evolution. *PLOS Genetics*, **11**(4):1–29.
- 719 The 1000 Genomes Project Consortium, 2015. A global reference for human genetic varia-
720 tion. *Nature*, **526**(7571):68–74.
- 721 Turchin, M. C., Chiang, C. W., Palmer, C. D., Sankararaman, S., Reich, D., Genetic
722 Investigation of, A. T. C., and Hirschhorn, J. N., 2012. Evidence of widespread selection
723 on standing variation in europe at height-associated snps. *Nat Genet*, **44**(9):1015–9.
- 724 Wang, T. J., Zhang, F., Richards, J. B., Kestenbaum, B., van Meurs, J. B., Berry, D.,
725 Kiel, D. P., Streeten, E. A., Ohlsson, C., Koller, D. L., *et al.*, 2010. Common ge-
726 netic determinants of vitamin d insufficiency: a genome-wide association study. *Lancet*,
727 **376**(9736):180–8.
- 728 Wilde, S., Timpson, A., Kirsanow, K., Kaiser, E., Kayser, M., Unterländer, M., Hollfelder,
729 N., Potekhina, I. D., Schier, W., Thomas, M. G., *et al.*, 2014. Direct evidence for

730 positive selection of skin, hair, and eye pigmentation in europeans during the last 5,000
731 y. *Proceedings of the National Academy of Sciences*, **111**(13):4832–4837.

732 Wood, A. R., Esko, T., Yang, J., Vedantam, S., Pers, T. H., Gustafsson, S., Chu, A. Y.,
733 Estrada, K., Luan, J., Kutalik, Z., *et al.*, 2014. Defining the role of common variation in
734 the genomic and biological architecture of adult human height. *Nat Genet*, **46**(11):1173–
735 86.

736 Yin, X., Low, H. Q., Wang, L., Li, Y., Ellinghaus, E., Han, J., Estivill, X., Sun, L., Zuo, X.,
737 Shen, C., *et al.*, 2015. Genome-wide meta-analysis identifies multiple novel associations
738 and ethnic heterogeneity of psoriasis susceptibility. *Nat Commun*, **6**:6916.

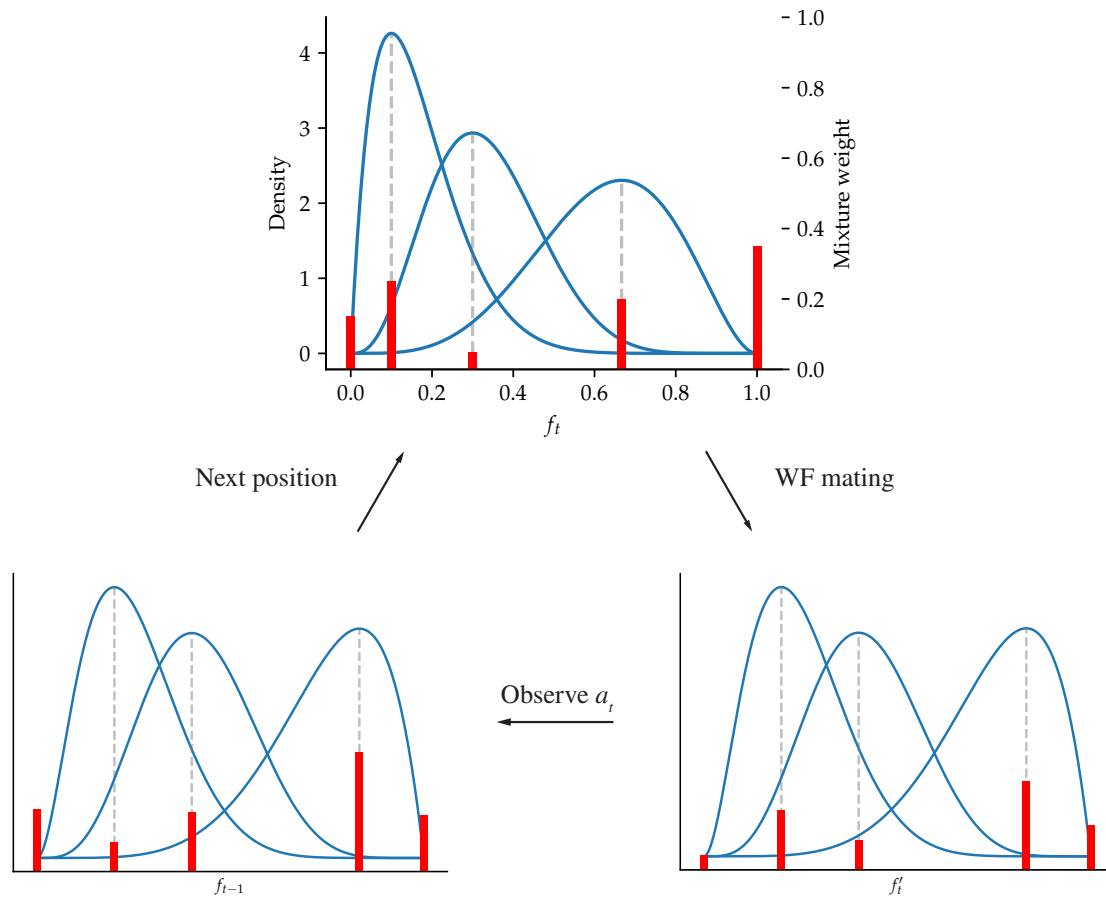


Figure 1: The BMwS model. At each time step t , the latent allele frequency f_t is modeled as a mixture of beta distributions, plus spikes at zero and one. In this diagram, there are $M = 3$ mixture components (blue lines). Mixture weights are indicated as red bars, including the spike weights p_0 and p_1 at $f_t = 0$ and $f_t = 1$, respectively. After Wright-Fisher mating, the shape of each beta mixture component, as well as the mixture weights, are updated according to equation (15). After observing the data a_t , the mixture weights are again updated according to Bayes' rule (equation 16). The process then iterates.

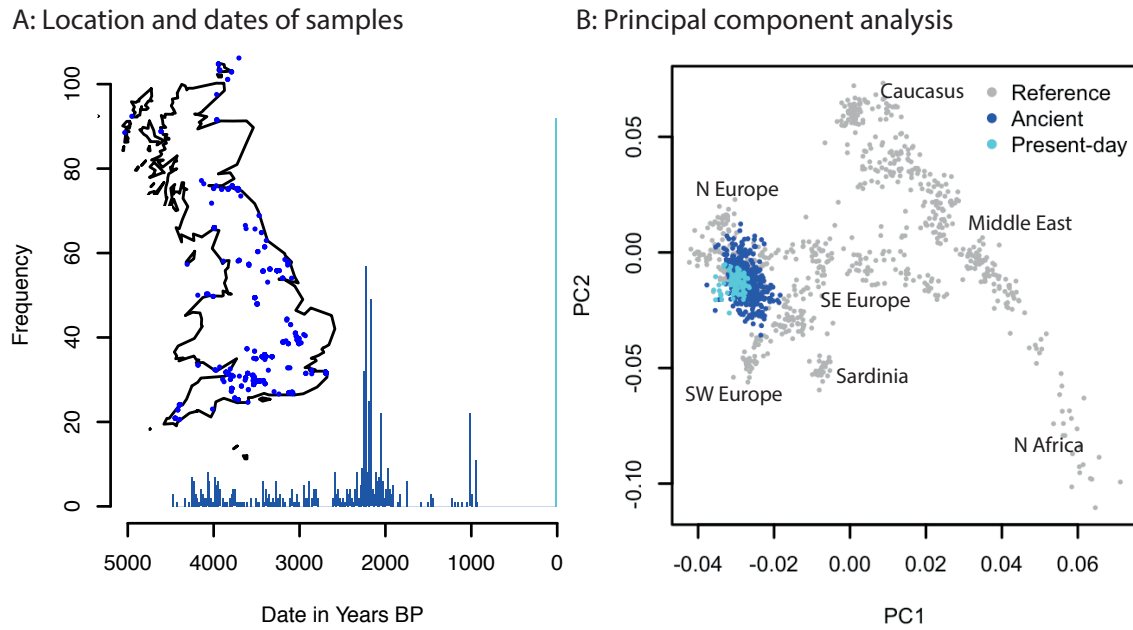


Figure 2: Ancient British data. **A**: histogram of dates of ancient individuals. Inset map shows locations of sites. **B**: Principal components of ancient and present-day samples projected onto axes defined by 777 West Eurasian individuals (see [Lazaridis et al. \(2014\)](#) for details of these individuals).

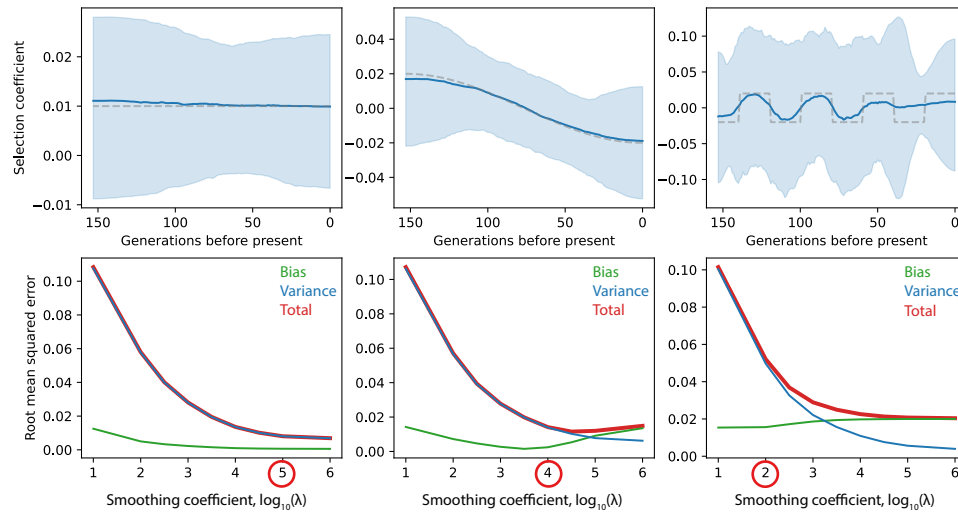


Figure 3: Simulation results for the sampling distribution of the ancient British data. Each column shows a different selection coefficient trajectory. **Upper row**: Estimated selection coefficients. Dashed line: simulated selection coefficient. Solid blue line: mean selection coefficient from 1000 simulations. Light blue shaded area: region containing point estimates from 950/1000 simulations. **Lower row**: Square root of squared bias, variance and total squared error as a function of $\log_{10}(\lambda)$. The circled value is the one used for the estimates in the upper row.

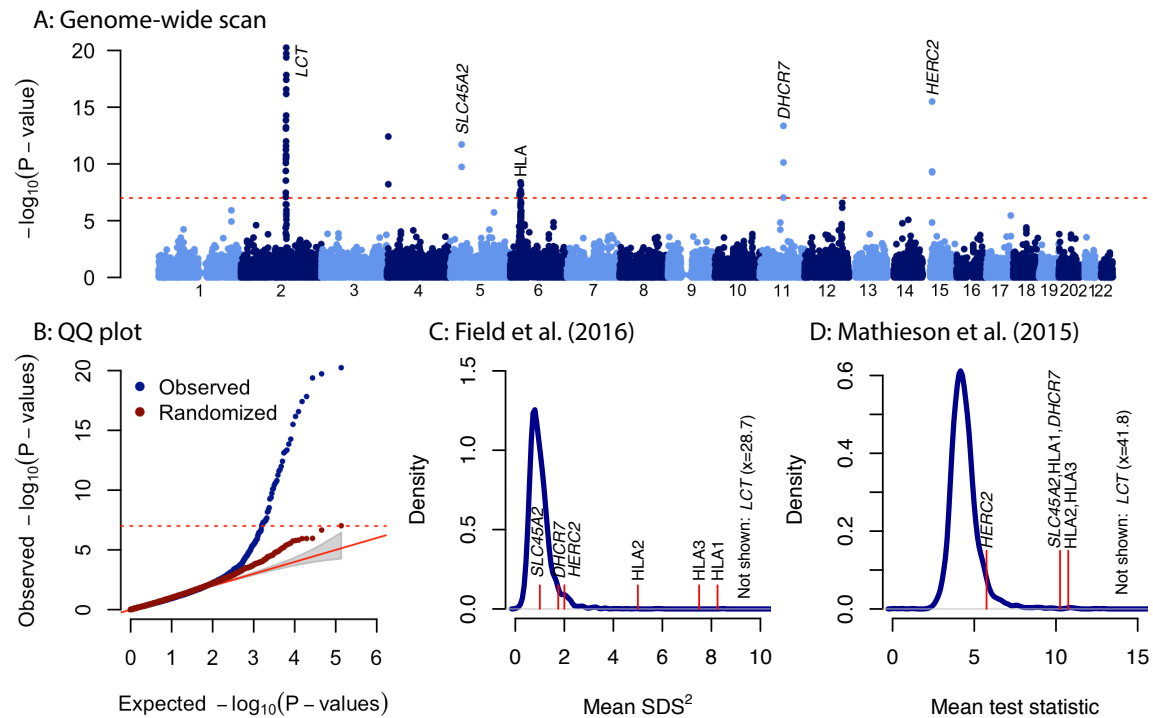


Figure 4: Genome-wide scan for selection in Britain **A**: P-values for selection in 20-SNP sliding windows. Genome-wide significant ($P < 10^{-7}$) windows are labeled with the closest gene or known target of selection. **B**: QQ plot for observations in **A** (blue) and after randomizing the dates of each sample (red). **C**: Comparison with results of [Field et al. \(2016\)](#). Blue solid line shows the density of mean SDS^2 in 20-SNP windows. Labeled red lines indicate windows that are genome-wide significant in our analysis. **D**: Comparison with results of [Mathieson et al. \(2015\)](#). Blue solid line shows the density of mean χ_3^2 statistic in 20-SNP windows. Labeled red lines indicate windows that are genome-wide significant in our analysis. In both **C** and **D**, *HERC2* is approximately at the upper 5th percentile of the distribution.

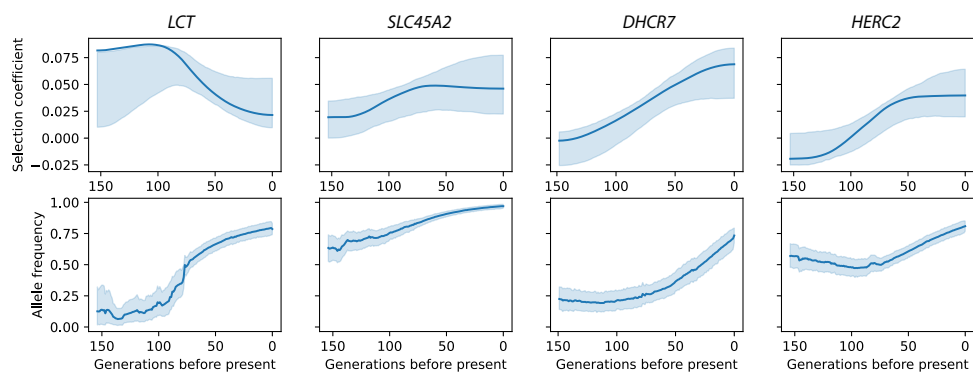


Figure 5: Trajectories of genome-wide significant non-HLA loci. Solid lines show the inferred selection coefficient and trajectory of the lead SNP given in Table 1. Shaded areas show 95% credible intervals based on resampling of the allele frequency trajectories and observations. Upper row: Estimated selection coefficients. Lower row: Estimated allele frequency trajectories.

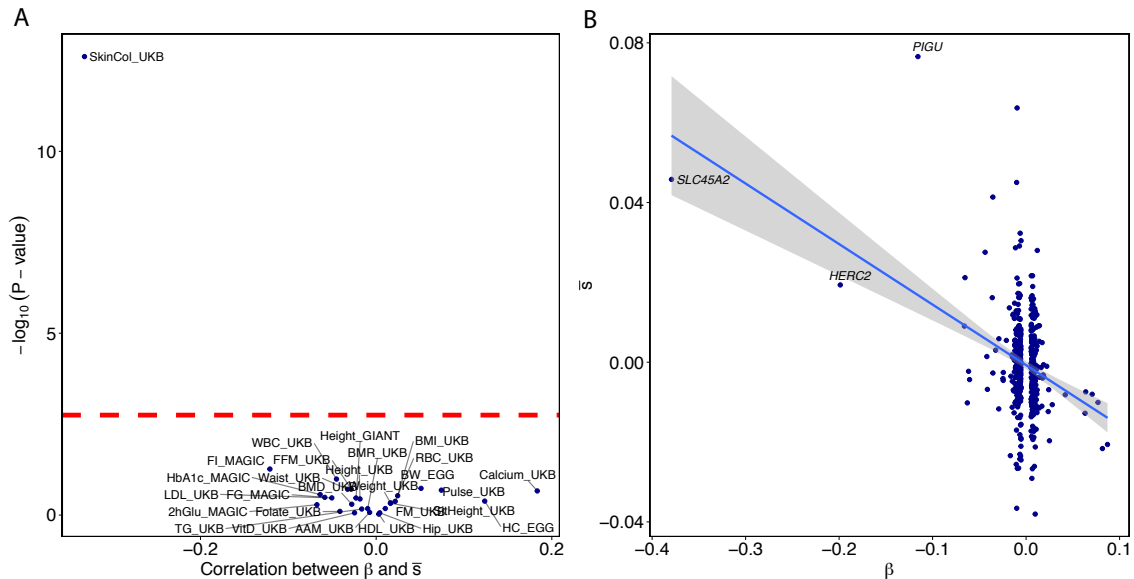


Figure 6: **A:** Evidence of polygenic selection. Each point represents a single GWAS. The x-axis gives the (Pearson) correlation between effect size estimates β and selection coefficient estimates \bar{s} for independent SNPs with GWAS P-value $< 10^{-4}$ and minor allele frequency $> 5\%$. The y-axis gives the \log_{10} (P-value) for null hypothesis of no correlation. Abbreviations, exact values and sources are given in Table S1. **B:** Effect sizes and selection coefficient estimates for independent skin colour associated SNPs in UK Biobank with GWAS P-value $< 10^{-4}$ and minor allele frequency $> 5\%$. If the three labeled large-effect SNPs are removed, the correlation is weaker but still significant ($\rho = -0.20$, $P=1.5 \times 10^{-5}$).